Optics Letters

Hybrid Hermite–Laguerre–Gaussian vector modes

EDGAR MEDINA-SEGURA,[1] LEONARDO MIRANDA-CULIN,[1] BENJAMIN PEREZ-GARCIA,[2] CARMELO ROSALES-GUZMÁN,[1,4] AND MITCHELL A. COX[3,*]

[1] *Centro de Investigaciones en Óptica, A.C., Loma del Bosque 115, Colonia Lomas del Campestre, 37150 León, Gto., Mexico*
[2] *Photonics and Mathematical Optics Group, Tecnologico de Monterrey, Monterrey 64849, Mexico*
[3] *School of Electrical and Information Engineering, University of the Witwatersrand, Johannesburg, South Africa*
[4] *carmelorosalesg@cio.mx*
[*] *mitchell.cox@wits.ac.za*

Received 7 November 2024; revised 10 December 2024; accepted 17 December 2024; posted 17 December 2024; published 15 January 2025

Vector modes are well-defined field distributions with spatially varying polarization states, rendering them irreducible to the product of a single spatial mode and a single polarization state. Traditionally, the spatial degree of freedom of vector modes is constructed using two orthogonal modes from the same family. Here, we introduce a novel class of vector modes whose spatial degree of freedom is encoded by combining modes from both the Hermite– and Laguerre–Gaussian families, ensuring that the modes are shape-invariant upon propagation. This superposition is not arbitrary, and we provide a detailed explanation of the methodology employed to achieve it. This new class of vector modes, which we term hybrid Hermite–Laguerre–Gaussian (HHLG) vector modes, gives rise to subsets of modes exhibiting polarization dependence on propagation due to the difference in mode orders between the constituent modes, while remaining eigenmodes of free space. To the best of our knowledge, this is the first demonstration of vector modes composed of two scalar modes originating from different families.

https://doi.org/10.1364/OL.544541

The Helmholtz paraxial wave equation, when solved in various coordinate systems, unveils shape-invariant families of optical fields that propagate freely in space, unlike arbitrary beams, which do not retain their intensity structure in propagation. Specifically, the common scalar solutions with uniform polarization—Hermite–Gaussian (HG), Laguerre–Gaussian (LG), and Ince–Gaussian (IG) modes—are derived from Cartesian, polar, and elliptical coordinates, respectively. These modes collectively form complete and orthonormal bases within an infinite Hilbert space, enabling any paraxial optical field to be represented as a complex superposition of these scalar modes. However, it is important to remark that a general solution expressed as an arbitrary superposition of the aforementioned paraxial modes does not evolve nicely upon propagation; i.e., it is not necessarily shape-invariant and may exhibit intricate changes during propagation.

The polarization of light, which occupies a two-dimensional vector space, typically involves linear and circular polarizations as its primary bases. Pure vector modes of light exhibit varying polarization states across their transverse plane and thus cannot be simply reduced to the product of a spatial mode and a polarization vector. Such vector modes are crafted through the superposition of two orthogonal optical fields (scalar modes) with corresponding orthogonal polarization states [1]. Following this principle, Hermite– and Laguerre–Gaussian vector modes [2], as well as other innovative structures such as vector Bessel beams [3], Airy vector beams [4], “classically entangled” Ince–Gaussian modes [5], helical Mathieu–Gauss vector modes [6], parabolic vector beams [7], parabolic accelerating vector waves [8], and the recent helico-conical vector beams [9], have been developed. These vector beams showcase distinctive properties that are leveraged in high-speed kinematic sensing [10], holographic optical trapping [11], visible light communications [12], mode division multiplexing [13], resilience against turbulence [14,15], and quantum optics communications [16,17].

Typically, the scalar optical fields that constitute these vector modes originate from the same family. However, this conventional approach is not necessarily a strict requirement. In our work, we introduce a novel class of optical vector modes, which we have named hybrid Hermite–Laguerre–Gaussian (HHLG) vector modes, by combining two scalar modes from distinct families. This superposition, incorporating orthogonal polarization states from the circular polarization basis, exploits a well-established expression that links HG and LG modes through their completeness property to identify compatible pairs of scalar modes [18–20]. This technique enables the creation of novel spatial phase, intensity, and polarization structures with stable propagation characteristics. Additionally, these structures can be engineered to exhibit polarization dependence on propagation, due to differences in mode orders between the constituent modes, with an example shown in Fig. 1.

The general mathematical expression for a vector beam $\mathbf{U}(\mathbf{r}_\perp, z)$ is as follows:

$$\mathbf{U}(\mathbf{r}_\perp, z) = \cos\theta \;\; u_1(\mathbf{r}_\perp, z)\hat{e}_R + e^{i\alpha}\sin\theta \;\; u_2(\mathbf{r}_\perp, z)\hat{e}_L, \quad (1)$$

where $u_1(\mathbf{r}_\perp, z)$ and $u_2(\mathbf{r}_\perp, z)$ are two orthogonal scalar optical fields, $\hat{e}_R$ and $\hat{e}_L$ are the circular right- and left-handed unitary polarization vectors, θ is a weighting factor, α is the inter-modal

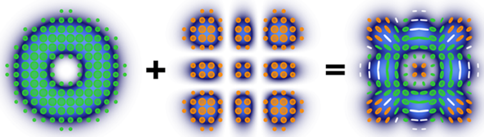

Fig. 1. Graphic representation of a HHLG vector mode employing LG_0^2 and $HG_{2,2}$ modes, with $\theta = \pi/4$ and $\alpha = 0$. Green ellipses illustrate right circular polarization, orange ellipses depict left circular polarization, and white lines indicate linear polarization states.

phase, z is the propagation coordinate, and $\mathbf{r}_\perp = (x, y) = (\rho, \phi)$ represents the transverse coordinate system. For the vector modes that we propose, $u_1(\mathbf{r}_\perp, z)$ is an optical field from the Laguerre–Gaussian basis, and $u_2(\mathbf{r}_\perp, z)$ is drawn from the Hermite–Gaussian basis, or vice versa. Thus, the mathematical expression for the HHLG vector modes is given by the following:

$$\mathbf{H}_{n,m}^{\ell,p}(\mathbf{r}_\perp, z) = \cos\theta \; LG_p^\ell(\rho,\phi,z)\hat{e}_R + e^{i\alpha}\sin\theta \; HG_{n,m}(x,y,z)\hat{e}_L, \tag{2}$$

where $HG_{n,m}$ and LG_p^ℓ are the orthogonal Hermite– and Laguerre–Gaussian modes. We will describe how to find these combinations later. In Cartesian coordinates, (x, y, z), the HG modes are defined as follows [21]:

$$\begin{aligned} HG_{n,m}(x,y,z) = &\sqrt{\frac{2}{\pi}}2^{-(m+n)/2}\frac{1}{\sqrt{n!m!w_0^2}}H_n\left[\sqrt{2}x/w(z)\right]\times \\ &H_m\left[\sqrt{2}y/w(z)\right]u_G(x,y,z)\exp[i\Psi_H(z)], \end{aligned} \tag{3}$$

where m and n are the indices of the mode, $H_m(\cdot)$ is the Hermite polynomial of order m, $w(z) = w_0\sqrt{1+(z/z_r)^2}$, $z_r = \pi w_0^2/\lambda$, and w_0 is the beam waist at the plane $z = 0$. $\Psi_H(z)$ is a propagation-dependent phase shift (described later), and

$$\begin{aligned} u_G(x,y,z) = &\frac{1}{\sqrt{1+(z/z_r)^2}}\exp\left[ik(x^2+y^2)/2R(z)\right]\times \\ &\exp\left[-(x^2+y^2)/w^2(z)\right] \end{aligned} \tag{4}$$

represents a Gaussian term, with $k = 2\pi/\lambda$ and $R(z) = z + z_r^2/z$.

Similarly, in polar cylindrical coordinates, (ρ, ϕ, z), the LG mode can be expressed as follows [21]:

$$\begin{aligned} LG_p^\ell(\rho,\phi,z) = &\sqrt{\frac{2p!}{\pi w_0^2(p+|\ell|)!}}\left(\frac{\sqrt{2}\rho}{w(z)}\right)^{|\ell|}\mathcal{L}_p^{|\ell|}\left(\frac{2\rho^2}{w^2(z)}\right)\times \\ &u_G(\rho,\phi,z)\exp(i\ell\phi)\exp[i\Psi_L(z)], \end{aligned} \tag{5}$$

where $\mathcal{L}_p^{|\ell|}(\cdot)$ is the Laguerre polynomial, p is the radial index, and ℓ is known as the topological charge. The phase term $\Psi_L(z)$ is a propagation-dependent phase shift, which will also be described later.

To create the HHLG vector modes, we must select modes from each family that are orthogonal. In order to identify orthogonal pairs of modes from the different families, we begin our analysis by expressing Laguerre–Gaussian (LG_p^ℓ) modes as linear combinations of Hermite–Gaussian ($HG_{n,m}$) modes [18–20]:

$$LG_p^l(\rho,\phi,z) = \sum_{k=0}^{N} i^k b(n,m,k)\mathrm{HG}_{N-k,k}(x,y,z), \tag{6}$$

obeying the index relations $n = (2p + |\ell| + \ell)/2$ and $m = (2p + |\ell| - \ell)/2$. The coefficients $b(n, m, k)$ of the superposition are

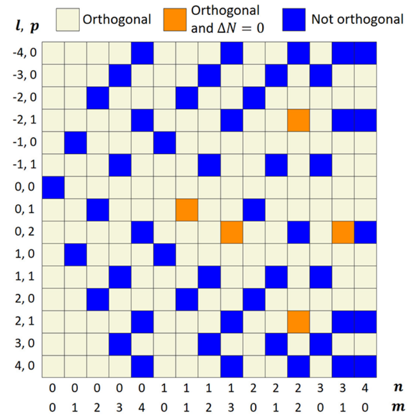

Fig. 2. For LG_p^l and HG_{nm} modes with $N_L, N_H \le 4$, there are 225 possible combinations. From these, 175 pairs of modes show orthogonality (beige) and five of them have the same mode order (orange).

given by the following:

$$b(n,m,k) = \sqrt{\frac{(N_* - k)!k!}{2^{N_*}n!m!}}\frac{1}{k!}\left[\frac{d^k(1-t)^n(1+t)^m}{dt^k}\right]_{t=0}, \tag{7}$$

where $N_L = 2p + |\ell|$ and $N_H = n + m$ is the mode order (generically N_*). The beam propagation factor, which describes the divergence of a beam, is simply $M^2 = N_* + 1$.

For different mode orders, orthogonality is guaranteed; however, there are cases where orthogonality occurs within the same N_*. For a given LG_p^ℓ mode, we first identify the equivalent combination of $HG_{n,m}$ modes and then select the remaining modes with the same order, i.e., where $b = 0$.

By way of example, we express the LG_1^{-2} as a linear combination of $HG_{n,m}$ modes by using Eqs. (6) and (7) as follows:

$$LG_1^{-2} = \frac{1}{2}HG_{4,0} + \frac{i}{2}HG_{3,1} + \frac{i}{2}HG_{1,3} - \frac{1}{2}HG_{0,4}. \tag{8}$$

Thus, we can conclude that LG_1^{-2} is *not* orthogonal to $HG_{4,0}$, $HG_{3,1}$, $HG_{1,3}$, or $HG_{0,4}$ because it is a linear combination of these modes. However, the remaining $N_* = 4$ mode, $HG_{2,2}$, must be orthogonal to LG_1^{-2} as it does not appear in Eq. (8).

In other words, any LG_p^ℓ is orthogonal to any $HG_{n,m}$ that does not appear in its Hermite–Gauss linear decomposition. Without loss of generality, we have restricted our analysis to a subset of modes where $N_* \le 4$, encompassing 15 $HG_{n,m}$ modes and 15 LG_p^ℓ modes. This leads to 225 possible combinations of modes as shown in Fig. 2. Within these combinations, 175 satisfy the orthogonality condition (beige color), including five pairs that share the same mode order (orange color). These five combinations, crucial to this new family of vector modes, are expected to preserve their non-homogeneous polarization patterns during propagation. Conversely, the polarization structure of the remaining 170 vector modes is anticipated to evolve predictably with propagation. The rate of this evolution will depend on the mode order difference, as is detailed below.

One might ask why not stay within a single basis and just use large superpositions? While conventional approaches such as mapping the HHLG mode into multiple LG or HG superpositions remain valuable, our technique offers a complementary perspective. By considering two distinct bases simultaneously, our method provides an elegant and insightful solution, offering an intuitive viewpoint.

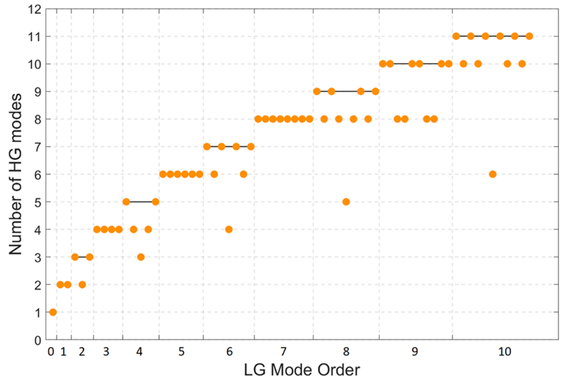

Fig. 3. Number of HG modes needed to obtain one single LG mode as a function of the LG mode order. Each point represents one LG mode and the horizontal axis is used to indicate the LG mode order.

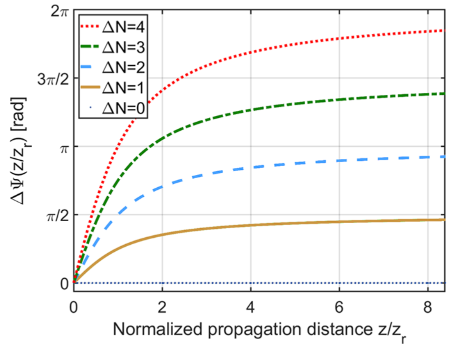

Fig. 4. Propagation-dependant phase difference $\Delta\Psi(z/z_r)$ of the hybrid Hermite–Laguerre–Gauss (HHLG) vector modes as a function of the normalized propagation distance z/z_r for different mode order differences ΔN.

Figure 3 illustrates the number of HG modes required to generate a single LG mode as a function of the LG mode order. In this graph, each point represents an LG mode, and the horizontal axis corresponds to its mode order. It is evident that as the mode order increases, the number of HG modes needed to obtain a single LG mode also rises.

An interesting interpretation of Fig. 3, based on Eq. (6), is that to obtain an LG mode of order N, $N + 1$ HG modes are required. However, some points in the graph, representing LG modes, deviate from this expected behavior. This can be explained by the fact that the coefficient b, calculated from Eq. (6), can be zero. Each time $b = 0$, the number of HG modes required is reduced by one.

For example, there are only three LG modes of order 2 (LG_1^0, LG_0^2, and LG_0^{-2}), and according to Eq. (6), the superposition of three HG modes should be needed to generate each of these LG modes. However, upon examining Fig. 2, we see that for the LG_1^0 mode, the mode $HG_{1,1}$ is orthogonal to it and shares the same mode order. This implies that only two modes are required to generate this particular LG mode instead of three.

This reasoning can be generalized to interpret all the LG modes in Fig. 3 that require fewer HG modes than their mode order plus one. These are the LG modes for which one or more orthogonal HG modes with the same mode order exist. Such special cases can be used to create hybrid vector modes that maintain their inhomogeneous polarization distribution during propagation.

As stated before, LG and HG modes have phase terms that depend on the propagation distance z, $\exp[i\Psi_L(z)]$ and $\exp[i\Psi_H(z)]$, respectively, where [1]

$$\Psi_L(z) = (2p + |\ell| + 1)\tan^{-1}(z/z_r) \equiv (N_L + 1)\tan^{-1}(z/z_r), \quad (9)$$

$$\Psi_H(z) = (n + m + 1)\tan^{-1}(z/z_r) \equiv (N_H + 1)\tan^{-1}(z/z_r). \quad (10)$$

Put simply, HHLG vector modes acquire a propagation-dependent phase difference given by the following:

$$\Delta\Psi(z/z_r) = \Delta N \tan^{-1}(z/z_r), \quad (11)$$

where $\Delta N = N_H - N_L$. For reference, Fig. 4 shows the phase difference $\Delta\Psi(z/z_r)$ as a function of the normalized propagation distance for different values of ΔN.

HHLG vector modes were experimentally generated through the coherent superposition of two orthogonal scalar modes with orthogonal polarization states in the circular basis, employing the experimental setup described in [22]. This setup utilizes a phase-only spatial light modulator (SLM) and a common path interferometer. While a detailed explanation of this technique lies beyond the scope of this Letter, it is worth mentioning that there are many other ways to generate them; nonetheless, we believe this method provides one of the highest stability. Additionally, Stokes polarimetry, as outlined in [23,24], was employed to measure the polarization distribution across the transverse plane of the vector modes at various z-planes, aiming to characterize their propagation behavior. To this end, we implemented the digital propagation method described in [25], based on the angular spectrum approach. This method allows for the calculation of the field distribution of a scalar mode at any arbitrary z-plane, $U(\mathbf{r}_\perp, z)$, as $U(\mathbf{r}_\perp, z) = \mathcal{F}_\perp^{-1}\{\mathcal{F}_\perp\{U(\mathbf{r}_\perp, 0)\}\exp(ik_z(\mathbf{k}_\perp)z)\}$, where $\mathcal{F}_\perp\{\cdot\}$ and $\mathcal{F}_\perp^{-1}\{\cdot\}$ denote the two-dimensional Fourier transform and its inverse, respectively; $k_z(\mathbf{k}_\perp)$ represents the wave vector component in the propagation direction. Experimentally, the required phase adjustments were applied using the SLM, and the inverse Fourier transform was performed using a biconvex lens with a focal length $f = 250$ mm.

We generated two examples of HHLG vector modes experimentally and measured their polarization distributions at various z-planes. The first, created through the superposition of $HG_{2,2}$ and LG_1^2 with equal weights ($\theta = \pi/4$ and $\alpha = 0$) in Eq. (2), showed no change in polarization distribution upon propagation, as evidenced in Fig. 5. Here, numerical simulations are presented in the left column and experimental results on the right. The beam's size increase due to diffraction is also visible. We computed the concurrence (sometimes called the vector quality factor) [26–28] to quantify the vector quality of the modes, finding excellent agreement between the simulations and experimental results. The second example involved the superposition of $HG_{0,7}$ and LG_1^1 with $\theta = \pi/4$ and $\alpha = 0$ in Eq. (2). The chosen spatial modes resulted in $\Delta N = 4$, a scenario not depicted in Fig. 2. We anticipated that this vector mode would acquire a phase difference between the constituent modes upon propagation, as described by Eq. (11), corresponding to the red dotted curve in Fig. 4. The overlaid polarization distribution and transverse intensity profile, shown in Fig. 6, reveal how the linear polarization states rotate from horizontal at $z = 0$ to vertical at $z = z_r$ through propagation.

Vector modes of light are becoming increasingly important due to their diverse applications and unique fundamental

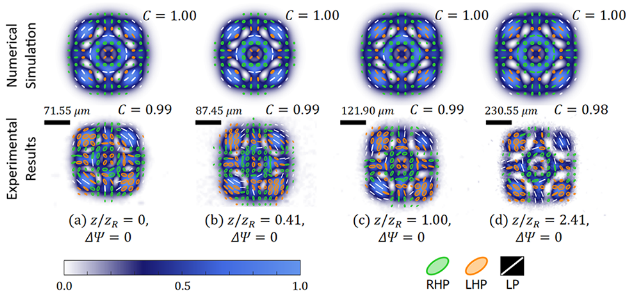

Fig. 5. HHLG vector modes for $w_0 = 0.6$ mm, $\lambda = 633$ nm, and mode parameters $l = 2,\ p = 1,\ n = 2,\ m = 2$ that result in $\Delta N = 0$ at different propagation distances: (a) $z/z_r = 0$, (b) $z/z_r = 0.41$, (c) $z/z_r = 1.00$, and (d) $z/z_r = 2.41$.

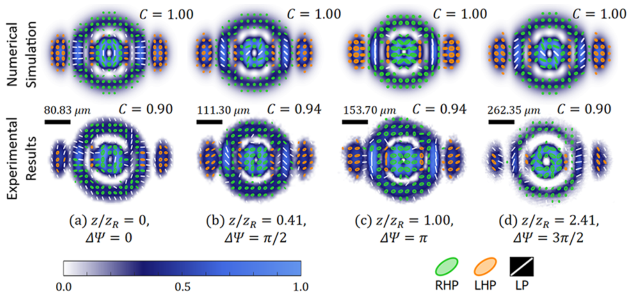

Fig. 6. HHLG vector modes for $w_0 = 0.6$ mm, $\lambda = 633$ nm, and mode parameters $l = 1,\ p = 1,\ n = 0,\ m = 7$ that result in $\Delta N = 4$ at different propagation distances: (a) $z/z_r = 0$, (b) $z/z_r = 0.41$, (c) $z/z_r = 1.00$, and (d) $z/z_r = 2.41$.

properties. In this study, we aim to contribute to the ongoing research on structured light by introducing a new type of vector mode. We do this with a novel and intuitive way of thinking about complex vector modes that are also eigenmodes of free space. "Complex" vector modes that propagate would normally require large superpositions from a single basis. We demonstrate that by carefully combining the spatial degrees of freedom from two different mode families into a single vector mode, we can create complexity while maintaining intuitive simplicity. Hybrid Hermite–Laguerre–Gaussian vector modes show interesting and configurable polarization behaviors during propagation, potentially forming "knots" or "bubbles" of polarization. We anticipate that other modal bases will produce equally fascinating results. While studies on scalar HHLG beams, such as their orbital angular momentum control using the radial index and their representation on the orbital Poincaré sphere [29], focus on scalar fields, these insights may provide a basis for exploring analogous behaviors here. Some speculative applications include a better understanding of modal diversity [20], where, for instance, one might wonder if the diversity gain emerges because of the modes themselves or the coherence between them, the concurrence of vector modes in turbulence and their use for FSO communications [15], where the addition of mode diversity in vector form might further improve the scheme leading to longer range and higher throughput wireless optical communications, novel optimized nonlinear frequency conversion through tailored pump modes [30], where "brute forcing" a particular spatial phase and intensity might be unnecessarily computationally intensive, and secure communications [31], where vector modes from different bases may add complexity and make it more challenging to intercept communications; potential beam shifts and surface interactions [32]; and perhaps new optical trapping capabilities [33].

Funding. National Research Foundation (TTK2204011621); Consejo Nacional de Humanidades, Ciencias y Tecnologías (EMS (CVU 742790), LMC (CVU 894875)).

Disclosures. The authors declare no conflicts of interest.

Data availability. Data underlying the results presented in this Letter are not publicly available at this time but may be obtained from the authors upon reasonable request.

Supplemental document. See Supplement 1 for supporting content.

REFERENCES

1. C. Rosales-Guzmán, B. Ndagano, and A. Forbes, J. Opt. **20**, 123001 (2018).
2. C. Maurer, A. Jesacher, S. Fürhapter, *et al.*, New J. Phys. **9**, 78 (2007).
3. A. Dudley, Y. Li, T. Mhlanga, *et al.*, Opt. Lett. **38**, 3429 (2013).
4. J. Zhou, Y. Liu, Y. Ke, *et al.*, Opt. Lett. **40**, 3193 (2015).
5. Yao-Li, X.-B. Hu, B. Perez-Garcia, *et al.*, Appl. Phys. Lett. **116**, 221105 (2020).
6. C. Rosales-Guzmán, X.-B. Hu, V. Rodríguez-Fajardo, *et al.*, J. Opt. **23**, 034004 (2021).
7. X.-B. Hu, B. Perez-Garcia, V. Rodríguez-Fajardo, *et al.*, Photonics Res. **9**, 439 (2021).
8. B. Zhao, V. Rodríguez-Fajardo, X.-B. Hu, *et al.*, Nanophotonics **11**, 681 (2022).
9. E. Medina-Segura, L. Miranda-Culin, V. Rodríguez-Fajardo, *et al.*, Opt. Lett. **48**, 4897 (2023).
10. S. Berg-Johansen, F. Töppel, B. Stiller, *et al.*, Optica **2**, 864 (2015).
11. N. Bhebhe, P. A. Williams, C. Rosales-Guzmán, *et al.*, Sci. Rep. **8**, 17387 (2018).
12. Y. Zhao and J. Wang, Opt. Lett. **40**, 4843 (2015).
13. M. A. Cox, N. Mphuthi, I. Nape, *et al.*, IEEE J. Sel. Top. Quantum Electron. **27**, 1 (2021).
14. M. A. Cox, C. Rosales-Guzmán, M. P. J. Lavery, *et al.*, Opt. Express **24**, 18105 (2016).
15. C. Peters, M. Cox, A. Drozdov, *et al.*, Appl. Phys. Lett. **123**, 21103 (2023).
16. B. Ndagano, I. Nape, M. A. Cox, *et al.*, J. Lightwave Technol. **36**, 292 (2018).
17. B. Ndagano, B. Perez-Garcia, F. S. Roux, *et al.*, Nat. Phys. **13**, 397 (2017).
18. M. Beijersbergen, L. Allen, H. van der Veen, *et al.*, Opt. Commun. **96**, 123 (1993).
19. A. T. O'Neil and J. Courtial, Opt. Commun. **181**, 35 (2000).
20. M. A. Cox, L. Cheng, C. Rosales-Guzmán, *et al.*, Phys. Rev. Appl. **10**, 024020 (2018).
21. G. Gbur, *Singular Optics* (CRC Press, 2016).
22. B. Perez-Garcia, C. López-Mariscal, R. I. Hernandez-Aranda, *et al.*, Appl. Opt. **56**, 6967 (2017).
23. K. Singh, N. Tabebordbar, A. Forbes, *et al.*, J. Opt. Soc. Am. A **37**, C33 (2020).
24. M. A. Cox and C. Rosales-Guzmán, Appl. Opt. **62**, 7828 (2023).
25. C. Schulze, D. Flamm, M. Duparré, *et al.*, Opt. Lett. **37**, 4687 (2012).
26. M. McLaren, T. Konrad, and A. Forbes, Phys. Rev. A **92**, 023833 (2015).
27. A. Selyem, C. Rosales-Guzmán, S. Croke, *et al.*, Phys. Rev. A **100**, 063842 (2019).
28. A. Manthalkar, I. Nape, N. T. Bordbar, *et al.*, Opt. Lett. **45**, 2319 (2020).
29. A. Volyar and M. Bretsko, J. Opt. Soc. Am. A **41**, 1648 (2024).
30. S. Singh, B. Sephton, I. Morland, *et al.*, J. Opt. Soc. Am. B **40**, 3128 (2023).
31. B. Ndagano, I. Nape, B. Perez-Garcia, *et al.*, Sci. Rep. **7**, 13882 (2017).
32. W. Zhen and D. Deng, Appl. Phys. B **126**, 35 (2020).
33. E. Otte and C. Denz, Appl. Phys. Rev. **7**, 041308 (2020).